MATERIALS SCIENCE

Locally controllable magnetic soft actuators with reprogrammable contraction-derived motions

Yahe Wu[1]†, Shuai Zhang[1]†, Yang Yang[2], Zhen Li[3], Yen Wei[1]*, Yan Ji[1]*

Reprogrammable magneto-responsive soft actuators capable of working in enclosed and confined spaces and adapting functions under changing situations are highly demanded for new-generation smart devices. Despite the promising prospect, the realization of versatile morphing modes (more than bending) and local magnetic control remains challenging but is crucial for further on-demand applications. Here, we address the challenges by maximizing the unexplored potential of magnetothermal responsiveness and covalent adaptable networks (CANs) in liquid crystalline elastomers (LCEs). Various magneto-actuated contraction-derived motions that were hard to achieve previously (e.g., bidirectional shrinkage and dynamic 3D patterns) can be attained, reprogrammed, and assembled seamlessly to endow functional diversity and complexity. By integration of LCEs with different magneto-responsive threshold values, local and sequential magnetic control is readily realized. Many magnetic actuation portfolios are performed by rationally imputing "logic switch" sequences. Meanwhile, our systems exhibit additional favorable performances including stepwise magnetic controllability, multiresponsiveness, self-healing, and remolding ability.

INTRODUCTION

Wireless magneto-responsive dry soft actuators with the capability of remote control and fast response have been extensively investigated in various domains such as biomedical and surgical tools, soft robotics, and aerospace (*1*–*6*). Because of the strong penetrating power of the magnetic field, this kind of actuator can be manipulated in confined and enclosed spaces (e.g., human body and sealed devices) where other stimuli-controlled actuation systems are inapplicable or very sophisticated to realize, making magnetic actuation particularly outstanding in this regard. Great efforts have been paid on developing magneto-responsive dry soft actuators with complex motions and dynamic three-dimensional (3D) structures in virtue of magneto-responsive soft composites that are typically composed of hard/soft-magnetic fillers and soft polymeric material matrix (*4*–*10*). Very recently, a series of actuators and devices with fascinating configurations and functions have been designed with reprogrammability deeply involved (*11*–*16*).

Reprogrammability refers to the ability to alter the functions repeatedly according to different needs, which has become one of the hallmarks for new-generation advanced actuators to enable versatility and adaptability (*6*, *17*, *18*). Reprogrammable soft actuators are especially suitable for working in continually changing conditions and performing multitask by one entirety (*6*). To date, for reprogrammable magnetic soft actuators, hard-magnetic composites (e.g., NdFeB/polymer composites) were almost invariably used as the material platforms (*12*–*16*). The oriented magnetic particles respond to the imposed directional magnetic field, inducing bending of the material matrix; the change of motions or structural geometry (i.e., reprogramming) comes out from the magnetization redistribution. On the basis of the basic bending, a lot of reconfigurable 3D architectures have also been acquired (*8*, *12*). Beyond that, there was only one exception using crystalline polymer networks as the matrix that can be programmed with reversible contractile motions besides bending (*11*). However, the reported actuation strain was not large enough (~6%), leading to the result that the designed motions were derived from bending as well.

For the current reprogrammable magnetic actuation systems, there are two vital issues that require neat solutions, which are the limited bending-based shape-morphing behaviors and difficulties in local and sequential magnetic control. Large-scale reversible contraction has not been achieved in any reported reprogrammable systems, not to mention other higher-level contraction-based motions such as bidirectional shrinkage, combined movements (e.g., elongation while bending), and dynamic raised fine patterns, which are all common motion modes in machines or living creatures (e.g., human muscle) (*19*–*21*). Actually, bending can also be realized through uneven shrinkage. With contraction-based motions, magnetic actuation modes can be largely expanded, and more sought-after motions can be evolved (*18*, *22*). The other problem regarding local and sequential magnetic control (i.e., controlling the movement of the targeted local part, while other parts remain unchanged unless activated) comes from the intrinsic limitation of the magnetic field. As magnetic fields cannot directly concentrate on the specific area just like light. It is very difficult to control the movement of different areas locally and sequentially by magnetic fields. This issue has also been regarded as one of the main drawbacks of magnetic soft actuators compared with photo-responsive ones despite their outstanding applicability in the enclosed space than others (*23*, *24*). With local controllability, not only magnetic actuation flexibility will be largely improved, but also a variety of sequential movements and functions can be performed by simply controlling the motions of different areas. Using magnetic shielding techniques or pony-sized magnetic field (which should be much smaller than the actuators) is a somewhat indirect solution to achieve local control but will lead to more elaborate fabrication and operation that may outweigh the gain (*25*).

In this work, magnetic soft actuators with versatile reprogrammable contraction-derived motions, in which the motions can be

[1]The Key Laboratory of Bioorganic Phosphorus Chemistry and Chemical Biology, Department of Chemistry, Tsinghua University, Beijing 100084, China. [2]Institute of Nuclear and New Energy Technology, Tsinghua University, Beijing 100084, China. [3]Xuesen Laboratory of Space Technology, China Academy of Space Technology, Beijing 100094, China. *Corresponding author. Email: jiyan@mail.tsinghua.edu.cn (Y.J.); weiyen@tsinghua.edu.cn (Y.We.)
†These authors contributed equally to this work.

locally and sequentially controlled by magnetic fields, are reported. It is enabled by taking both the obvious and hidden advantages of combining magnetic responsiveness and covalent adaptable networks (CANs) in liquid crystalline elastomer (LCE) actuators. LCEs are an outstanding category of soft shape-morphing materials (*26*–*30*). They can convert external stimuli into various substantial reversible actuation after installing suitable alignment of mesogens (by mechanical alignment, surface alignment, 3D printing, compressive buckling, etc.) (*31*–*35*). Although there were sporadic cases regarding magnetic LCE actuators reported, none of them can be reprogrammed, and the motions were very simple (*36*–*39*). The benefits of introducing magneto-responsiveness into CAN-based LCEs had not been explored in the past. Here, magnetothermal-responsive [i.e., showing magnetothermal effect under alternating magnetic fields (AMFs)] polyurethane (PU) LCE (M-PULCE) actuators with dynamic carbamate bonds were developed to demonstrate our strategy (Fig. 1A). As illustrated in Fig. 1B, our materials are easy to build plenty of different magneto-responsive motion modes including large-scale tunable contraction (~80%), biaxial shrinkage, spiraling while elongating, complex dynamic 3D patterns, and so on more than bending. Moreover, local and sequential magnetic control of different parts in one monolith is achieved. The principle behind is different from light-enabled local control that benefits from the focused optical source (e.g., laser beams). Local magnetic control here is enabled by means of welding M-PULCEs with different contents of magnetic particles via AMF (Fig. 1C). With proper layout of different M-PULCEs at the required regions, only when the intensity of AMF reaches the predetermined value, subareas will be actuated correspondingly, which is similar to setting and controlling "logic switches." On the basis of this, we designed dexterous magnetic soft actuators that can be partially controlled and output abundant motion sequences by adjusting the input magnetic intensity.

Besides, there are additional merits highly desired for new-generation soft actuators realized by our strategy. First, in our system, dynamic covalent bond exchange can be activated by AMF, so seamless assembling of either bulks (hard to be welded by heat or light) or thin sheets can be achieved via AMF-assisted welding (*40*). Various magneto-controlled actuators composed of multiple materials with sophisticated heterogeneous structures were also built (Fig. 1D). Second, we found that M-PULCEs exhibited unique supercritical behaviors so that we can stepwise control the contraction-based motions magnetically. A great deal of intermediate motions can be supplemented for controllable magnetic actuation. Third, our materials are multistimuli responsive simultaneously in response to heat, light, and magnetic fields. Programming, actuating, motion erasing, and reprogramming processes can be enabled by these three stimuli. Furthermore, M-PULCEs exhibit good self-healability under AMF and light, and the used or broken actuators can be remolded into a renewed polydomain LCE film by hot pressing. Given that, we can make full use of the advantageous characteristics of our systems and pick the suitable set from the "toolbox" to build advanced magnetic soft actuators.

RESULTS

M-PULCEs were prepared by dispersing Fe_3O_4 nanoparticles (NPs) into PULCEs, CAN-based LCEs with exchangeable dynamic carbamate bonds. Fe_3O_4 NPs exhibit high magnetothermal conversion rates under the action of AMF and are commercially available (*41*, *42*). It was found that Fe_3O_4 NPs were well distributed in common PU systems in our previous work (*40*). To obtain M-PULCEs with favorable large-scale shape deformations, we prepared liquid crystal (LC) oligomers to decrease the cross-link density and prolong the chain length of the LC moieties. The hydroxyl-terminated LC oligomer

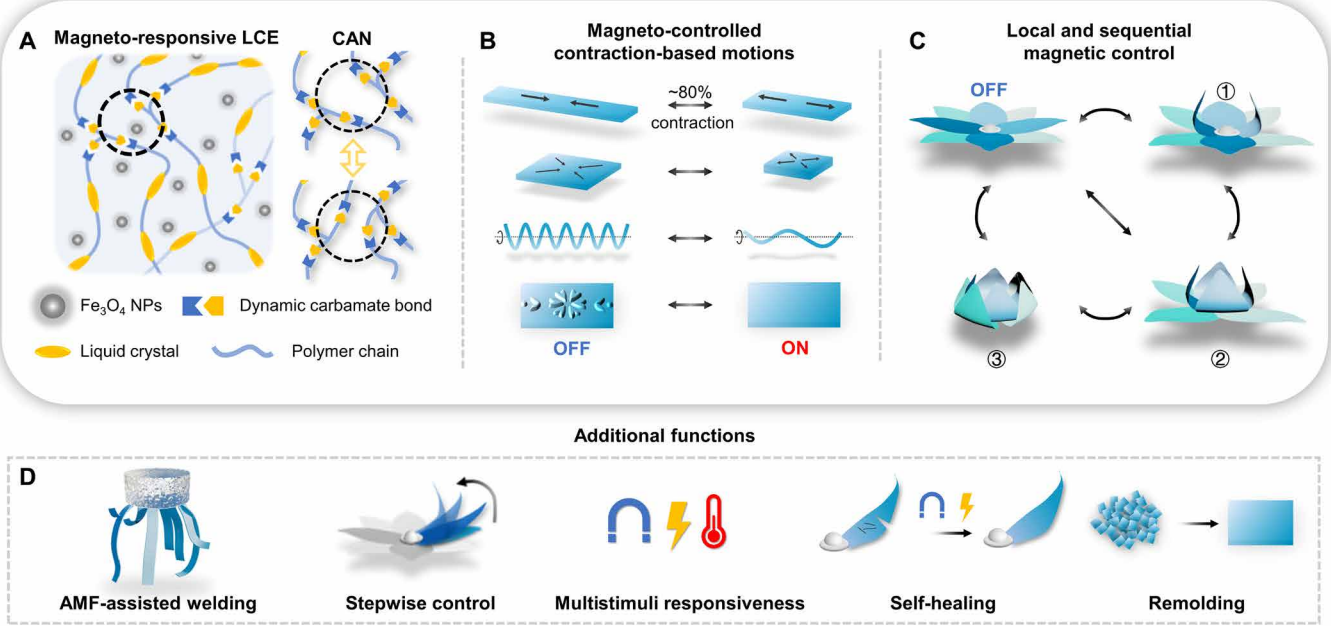

Fig. 1. Scheme of the reprogrammable magnetic LCE actuation system. The strategy of combining magnetothermal responsiveness with CAN in LCEs (**A**) to fabricate reprogrammable magnetic soft actuators with diversiform contraction-based motions (**B**) and local and sequential magnetic controllability (**C**). The strategy also brings additional favorable functions to the reprogrammable magnetic actuators including AMF-assisted welding, stepwise magnetic controllability, multiresponsiveness, self-healing, and remolding ability (**D**).

with an average molecular weight of about 4700 g/mol was prepared by RM82 (1,4-Bis-[4-(6-acryloyloxyhexyloxy)benzoyloxy]-2-methylbenzene) (a commercially available LC monomer), dithiol, and mercaptoethanol through a thiol-Michael addition reaction. A three-arm isocyanate was used as the cross-linker, and dibutyltin dilaurate (DBTDL) was used as a catalyst for polymerization and cross-linking. PULCEs with exchangeable carbamate bonds were then synthesized by the classic reaction between alcohol groups and isocyanates (Fig. 2A) (*43*, *44*). Superparamagnetic Fe_3O_4 NPs with a diameter of 20 nm were added into PULCEs before cross-linking [the content of Fe_3O_4 NPs: 5, 10, and 15 weight percent (wt %)]. The synthesized materials with 5, 10, and 15 wt % Fe_3O_4 NPs are abbreviated to M-PULCE-1, M-PULCE-2, and M-PULCE-3, respectively. Blank PULCEs without Fe_3O_4 NPs doped were also prepared as a control. Swelling experiments suggest that all the above samples have high gel contents, confirming their thermosetting nature (table S1 and fig. S2). According to differential scanning calorimetry (DSC) curves, the glass transition temperature (T_g) of blank PULCEs is about −11.4°C, and the LC-isotropic transition temperature (T_i) is about 99.5°C. Both T_g and T_i are rarely affected by adding Fe_3O_4 NPs, only showing a slight increase compared with the blank ones. T_i of M-PULCEs is between 101° and 105°C (fig. S3). The mechanical properties of M-PULCEs are fairly good. On the basis of the stress-strain tests, the elongation strain at break is in the range of 409 to 463%, while the breaking stress is in the range of 27 to 29 MPa (fig. S5).

Because of the presence of CAN, M-PULCEs can be readily aligned and realigned (i.e., reprogramming) through heat-induced network rearrangement (*17*, *31*). Under the catalysis of DBTDL, transcarbamoylation will be induced at elevated temperatures (Fig. 2B) (*44*). A 150°C was chosen as the programming and reprogramming temperature in consideration of the moderate relaxation rate (figs. S6 and S7). Monodomain M-PULCEs and blank PULCEs with reversible contraction were fabricated according to the following process. The as-prepared polydomain LCE sample was uniaxially stretched to 180% of its original length; the alignment was fixed through network topological change at 150°C; an actuator with reversible contraction motions was the outcome (*17*). Upon heating, the monodomain sample goes through the LC-isotropic transition, leading to a contraction process, while after cooling, it reverts to the LC phase and elongates (*45*, *46*). The uniaxial alignment of PULCEs and M-PULCEs was verified through polarized optical microscope (POM) and 2D x-ray diffraction (XRD) tests (fig. S8).

The programmed motions can be controlled by AMF due to the introduction of Fe_3O_4 NPs (*41*). The magnetic actuation of M-PULCEs originates from the comprehensive effect of both LCE and the magnetothermal effect of Fe_3O_4 NPs. As schematized in Fig. 2C, under AMF, Fe_3O_4 NPs convert the energy of AMF into heat on account of the hysteresis loss, relaxation loss, and other factors, resulting in a quick temperature increase of the aligned LCE composites; when the temperature reaches T_i of LCEs, the polydomain-monodomain transition are triggered, so the actuation will perform. In this regard, we tested the magneto-responsive characteristics in AMF of M-PULCEs with different contents of Fe_3O_4 NPs. Under a certain AMF (constant intensity H and frequency f), similar to the findings in our previous findings, higher content of Fe_3O_4 NPs determines the higher final temperature and the faster heating rate, which were characterized by an infrared (IR) thermographic camera (*40*).

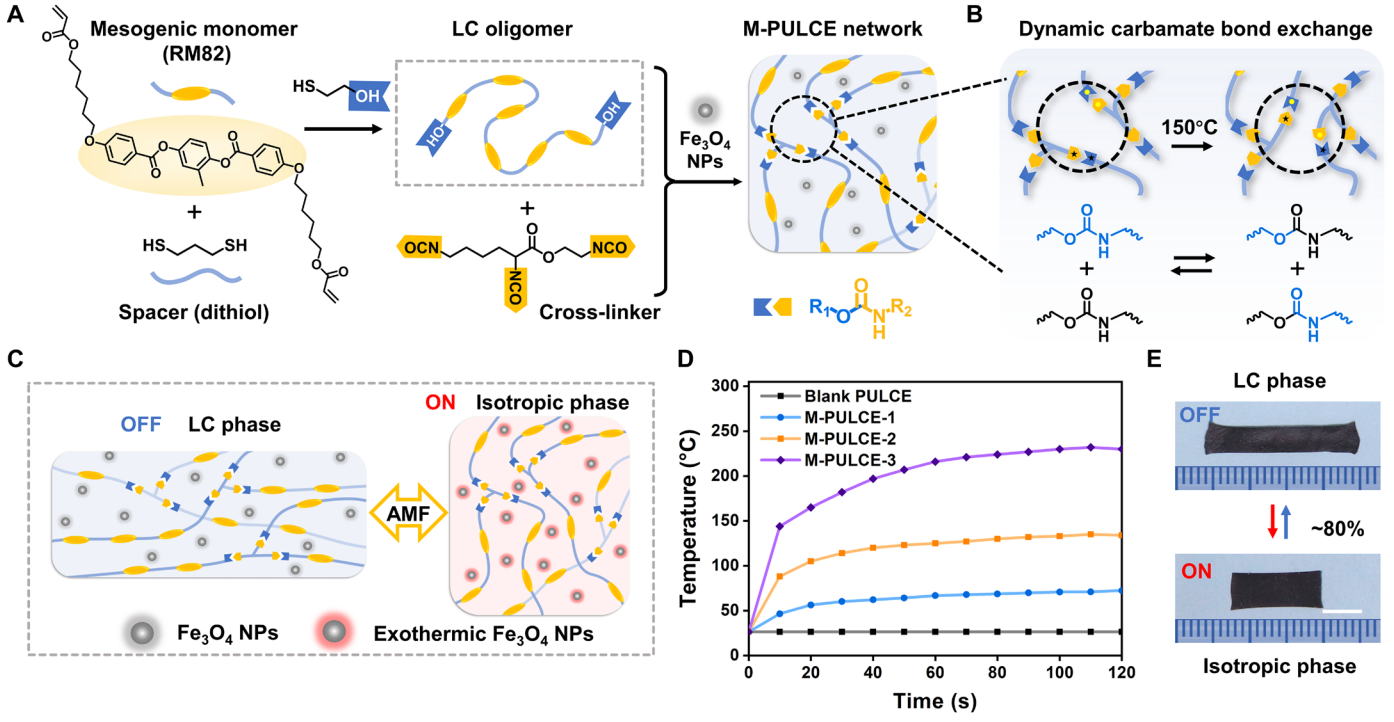

Fig. 2. M-PULCE actuators with dynamic carbamate bonds. (**A**) Synthesis of M-PULCEs. (**B**) Dynamic carbamate bond exchange. (**C**) Schematic illustration of the actuation mechanism of the aligned M-PULCE under AMF. (**D**) Heating curves of M-PULCEs and the blank PULCE with different contents of Fe_3O_4 NPs under AMF (f = 495 kHz, H = 166.79 Gs). M-PULCE-1, 5 wt % Fe_3O_4 NPs; M-PULCE-2, 10 wt % Fe_3O_4 NPs; M-PULCE-3, 15 wt % Fe_3O_4 NPs. (**E**) Images of the uniaxially aligned M-PULCE (i.e., monodomain) showing reversible contraction between LC phase (30°C, AMF OFF) and isotropic phase [120°C, AMF ON (f = 320 kHz, H = 219.27 Gs)]. Scale bar, 5 mm.

Specifically, in the AMF with f = 495 kHz and H = 166.79 G, the temperature of M-PULCE-1 reached the upper limit of temperature 75°C in about 2 min; for M-PULCE-2, the material was heated up to the stable temperature, 130°C, in 60 s, which would cause the LC-isotropic transition for magnetic actuation; for M-PULCE-3, the final temperature is about 230°C; as a control, the temperature of the blank PULCE did not change at all (Fig. 2D).

Under AMF, the maximum contractile strain of M-PULCEs reaches ca. 80% (obtained by M-PULCE-2), much larger than that of the previously reported reprogrammable magnetic dry soft actuators (Fig. 2E, table S2, and fig. S8). In the context, without specific descriptions, M-PULCE-2 was used as the prototype for most characterizations and demonstrations. The contractile strain (also called actuation strain in the context) is defined as $(L_0 - L_i) / L_i$ (L_0 is the length of the uniaxially aligned LCE in the LC phase at about 25°C, and L_i is the length in the isotropic phase above T_i). The reversible large-scale contraction is very essential in lots of devices for doing work. For instance, in artificial muscle, a long-lasting hot topic, reversible large-scale contraction is the inevitable motion and in great demand (*7*, *19*). Higher actuation stain indicates a better capacity for larger mechanical work output (for human skeletal muscle, the actuation strain is about 40%). However, now large-scale reversible contraction had not been attained in magneto-actuated soft actuators with favorable reprogrammability; the reported highest contraction value is only about 6% (*11*). We have expanded this value by 13 times in this work. The repeated actuation cycle curves of the monodomain M-PULCE-2 also showed the competent actuation stability under AMF (fig. S9). The magnetic field is an excellent power source, able to penetrate the surface of the object (except for magnetic shielding material) and act on the targeted responsive material inside without injuring other non–magnetothermal-responsive parts, which can hardly or is very sophisticated to be achieved by other stimuli such as light and heat (*1*, *25*). As illustrated in Fig. 3A, a composite M-PULCE film with reversible contraction motion can be built as an artificial muscle in the sealed robotic arm. When AMF is applied, the magnetic field can activate the movements of the M-PULCE that acts on the whole mechanical arm, making the arm up and down wirelessly. The external shell can effectively protect the core actuators, slow down the damage, and prolong its service life, thereby promoting its further applications.

Besides the basic large-scale contraction, we flexibly established various magneto-controlled contraction-derived motions by M-PULCEs. Unlike other reprogrammable magnetic actuators, the complex shape deformation of which is simply set by bending, M-PULCEs can be programmed with diversified geometry and movements by using suitable external forces or molds. In this LCE system, the magneto-responsive motion modes depend on the mesogen order patterns (*47*). We set examples including spiraling while elongating, coiling/uncoiling, and bidirectional shrinkage, which were very difficult to manufacture in reprogrammable magnetic actuators previously for demonstration (Fig. 3B; see Materials and Methods for detailed preparation procedures). For instance, the bidirectional shrinkage motion was obtained by bidirectionally stretching a polydomain M-PULCE rectangular film along the two diagonal lines to a certain strain and fixing the alignment at 150°C. The shrinkage ratio along the diagonal lines can be regulated by simply altering the stretching strain. We also constructed a 3D convex (Fig. 3C) and dynamic 3D patterns (Fig. 3D) that reversibly vanish/arise upon AMF ON/OFF, applicable for Braille display, anticounterfeit, and so on (*48*, *49*). On the basis of the reversible coiling/uncoiling motion and the synergetic magnetic responsiveness, a simple demonstration of the M-PULCE actuator for transporting and releasing objects inside/through an opaque tube is displayed here (Fig. 3E). An object was first entangled within the spiral-shape actuator under AMF. Apart from magneto-thermal responsiveness, M-PULCEs also can be manipulated by permanent magnets because of the superparamagnetic property of the added Fe_3O_4 NPs (*50*). Under the guidance of the permanent magnet, the M-PULCE actuator with the "cargo" rolled forward and passed into the opaque tube. At the required site inside the tube, the cargo can be released from the actuator by switching on the AMF; after that, once the AMF was turned off, the permanent magnet was moved back immediately for pulling the actuator away from the cargo; the actuator coiled again during the moving process and was ready for the next task.

The programmed motions can be recomposed at will. The reprogrammability is an intrinsic feature of our M-PULCEs because of the dynamic carbamate bonds (*17*). For demonstration, a contractile actuation was initially "written" into the M-PULCEs (strictly speaking, this progress can also be considered as reprogramming), since there was no actuation at all for the as-prepared completely cured M-PULCEs (i.e., polydomain samples); the contractile actuator was reconfigured into a helix-shape actuator showing a winding/unwinding motion under AMF (fig. S10). An actuation erasing process can also be introduced, which is particularly useful in many practical conditions, resembling "restore the factory default settings." It is enabled by allowing rearrangement of the cross-linked network at the isotropic phase to fix the disordered state, and the LCE will go back to the original polydomain state.

By CAN-enabled welding, magneto-controlled actuators with more complex geometry and integrated functions can be nicely designed and fabricated (*51*, *52*). Bond exchange can be activated by AMF, which facilitates magnetic welding. AMF-assisted welding is a more powerful tool in regards to assembling the covered interfaces (e.g., the overlapped site) and solid-core bulks in comparison with light and heat because of the strong penetrability (*16*). For successful welding, two materials were overlapped on the assigned region, and a certain external force was applied to make the overlapped site well contacted; the seamless welding was achieved by placing the sample in the AMF to trigger rearrangement of CANs (fig. S11). AMF-assisted welding is quite efficient. Once the temperature of M-PULCE reaches the fast bond exchange temperature (150°C) via magneto-caloric effect, only 5 min is required for complete welding of samples. We tested the reliability of the AMF-assisted welding process through lap-shear tests (fig. S11). The results showed that the magnetic welding is effective, and the welded sample did not fail after being stretched at more than 400% strain. This AMF-assisted processing is also applicable to microscale M-PULCEs. M-PULCE fibers (width: 160 μm; thickness: 120 μm) can also be successfully soldered (fig. S12). The process to build assembled actuators can be conducted by two methods. One is to complete the motion reprogramming while welding. The other is to weld the already programmed actuators by using solder with higher content of magnetothermal NPs to achieve selective welding on the aimed areas. By this method, under a suitable intensity of AMF, only the welding areas reached the activation temperature for bond exchange, while the actuation parts stayed at a lower temperature such that the programmed functions of these parts would not be destroyed by random bond exchange in the welding time scale (the detailed experimental

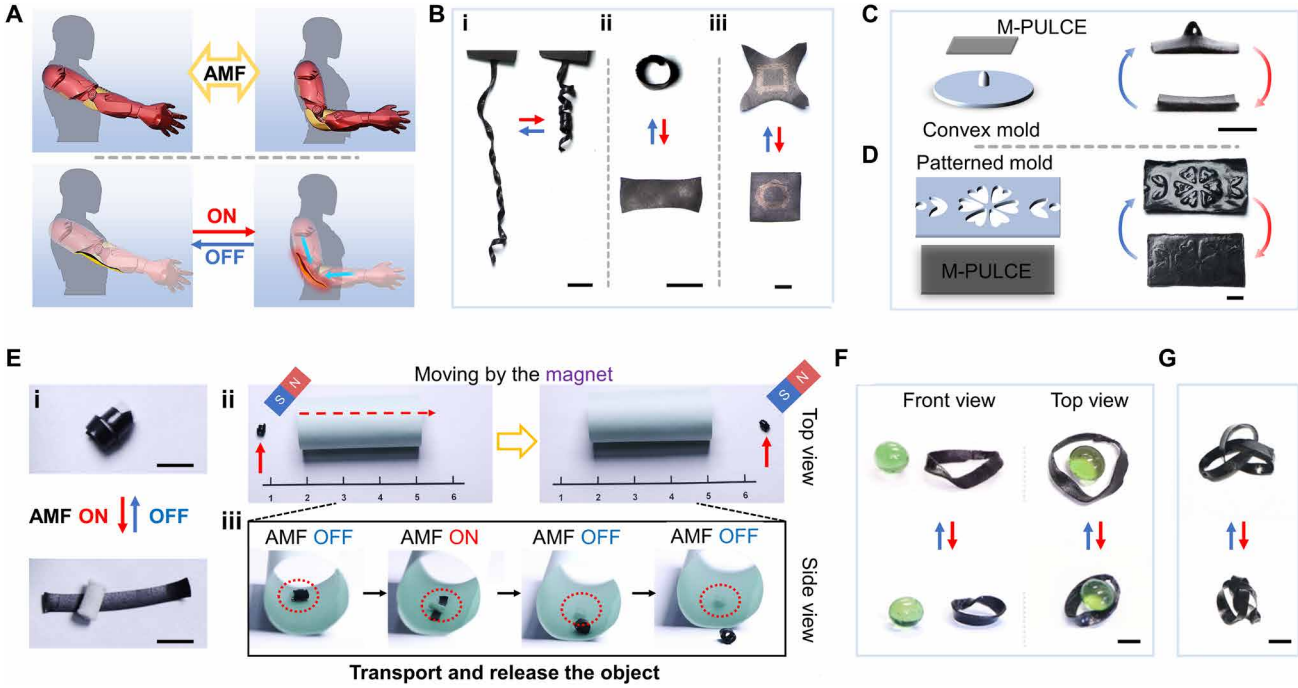

Fig. 3. M-PULCE actuators with diverse contraction-derived motions. (**A**) Illustration of the wireless magnetic actuation in the enclosed robot arm. The actuator performs a contraction motion under AMF, driving the artificial elbow to curve. (**B**) Various actuation motion modes of M-PULCEs under AMF. (i) Spiraling while elongating, (ii) coiling/uncoiling, and (iii) bidirectional shrinkage. (**C**) A 3D convex. (**D**) Dynamic patterns. (**E**) Transporting and releasing an object inside an opaque tube by an M-PULCE actuator with coiling/uncoiling motions. (i) The object can be entangled and released by the actuator under AMF. (ii) The actuator with the object rolling forward under the guidance of a permanent magnet along the tube. (iii) In the tube, the object was released (AMF ON); after that, the AMF was turned OFF, and the M-PULCE was moved out by the magnet immediately during recoiling; and then the actuator was moved away by the magnet. (**F**) Mobius ring with variable areas (AMF ON, diameter, d_1, area inside the ring, S_1; AMF OFF, diameter, $1.7d_1$, area, $2.9S_1$). (**G**) Contractible trefoil knot. In the above figures, the red arrow denotes turning on AMF, and the blue arrow denotes turning off AMF. All the motions were performed between 30° (AMF OFF) and 120°C (AMF ON, $f = 320$ kHz, $H = 219.27$ Gs). M-PULCE-2 was used for all the demonstrations. Scale bar, 5 mm.

procedures can be found in Materials and Methods). For complex geometry, the welding technique was used to build the structure that cannot be acquired by molding such as Mobius ring with variable areas (Fig. 3F) and trefoil knot (Fig. 3G). For diverse functions, we fabricated multifunctional 3D reprogrammable actuators, where the magnetically actuated bending/unbending motion, twisting/flattening motion, and coiling/uncoiling motion were joined together so that different parts can simultaneously carry out different tasks (Fig. 4A).

Moreover, not only can M-PULCEs be welded together, but also they can be welded with chemically different materials such as common PU materials (without LC moieties) to construct multicomponent actuators whether for the bulk materials or sheets by AMF-assisted welding. The "assembly" of extra components brings in more on-demand functions and physical properties into soft actuators, especially for the introduction of bulk materials (*43*, *53*). Bulk materials (including foams) can provide mechanical support, shock resistance, and other additional unique features, while their welding into magnetic soft actuators had not been achieved so far. PU foam can be easily welded with M-PULCEs via AMF. The successful welding and the strong bonding were verified by swelling test and lap-shear tests (fig. S13). The welded region remained well connected during and after swelling. After being stretched until fracture, the break occurs at the body of the PU foam rather than the welded joint. Notably, as we investigated previously, bulk CAN materials cannot be welded together by direct heat because the heating will act on all the samples, leading to the overwhelming shape destruction under pressure. Light is also very difficult to work on welding bulks, as the overlapped regions are covered by the thick "body" of the bulk material, making light blocked (*40*). By AMF-assisted welding, we fabricated monolithic magneto-responsive multimaterial actuators with heterogeneous structures (experimental details can be found in Materials and Methods). As shown in Fig. 4B, a satellite-like actuator was built by common PU CAN sheets and an M-PULCE hinge. This structure can be closed automatically under AMF and expanded after switching off the magnetic field, well simulating the process of folding/unfolding the battery panels in the satellite (movie S1). An artificial octopus was also made by assembling a PU CAN foam as the "head" with eight M-PULCE "legs" showing reversible curling or rolling motions (Fig. 4C and movie S2). With the foam head, this octopus-like actuator can float up after being pressed into the water many times, whereas the actuators of the same weight without the welded foam soon sank to the bottom (movies S3 and S4).

While reprogrammable magnetic actuators with different parts showing different functions are developed, a vital and unavoidable issue was raised, that is, can we also magnetically actuate the motion of the appointed part/parts locally and sequentially? So far, it is extremely difficult to achieve local control completely with a magnetic field. Previously localized and sequential motions have been commonly achieved by light-controlled systems (*54*, *55*). Nevertheless,

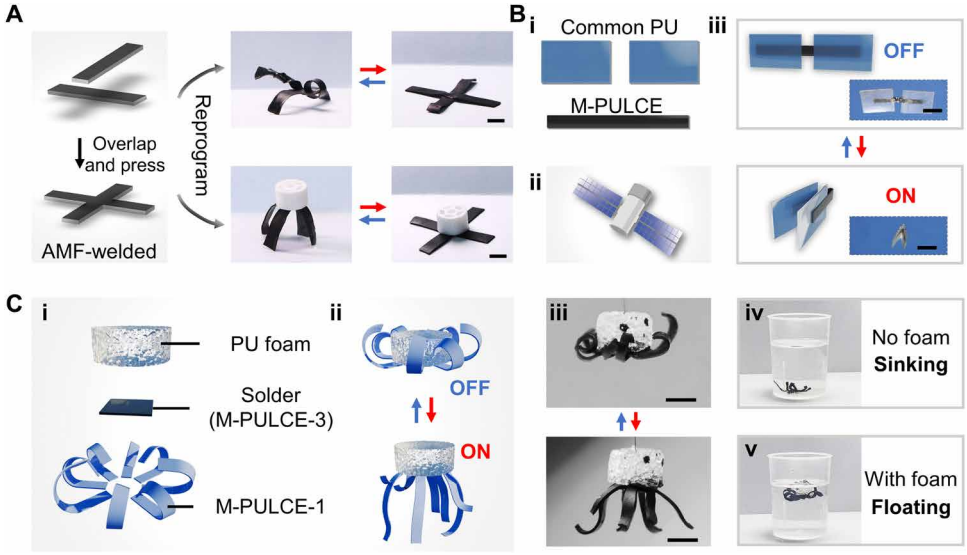

Fig. 4. Multifunctional and multimaterial magnetic soft actuators prepared by AMF-assisted welding. (**A**) Integrated M-PULCE-2 actuator with bending/unbending motion, twisting/flattening motion, and coiling/uncoiling motion and its reprogramming. AMF condition: $f = 320$ kHz, $H = 219.27$ Gs. (**B**) Multimaterial satellite-like soft actuator. (i) Before assembly (two "wings" and the hinge are made of common PU CANs and M-PULCE-2, respectively), (ii) the archetype of satellite, and (iii) assembled soft actuators with two "wings" closed when AMF is ON (inset: images). AMF condition: $f = 320$ kHz, $H = 219.27$ Gs. (**C**) Multimaterial octopus-like soft actuator. (i) Before assembly (the cylindrical head is composed of PU foam, the solder is M-PULCE-3, and the legs are made of M-PULCE-1), (ii) assembled soft actuators with eight legs straightening when AMF is ON, (iii) images of the assembled soft actuators, (iv) the M-PULCE actuator without the welded foam sinking in the bottom, and (v) assembled multimaterial soft actuators floating on the water. AMF condition: $f = 320$ kHz, $H = 283.15$ Gs. Scale bars, 10 mm.

as light is a contact-type stimulus and shows very limited penetration depth (for actuators, the penetration depth of near-IR (NIR) light is typically at the millimeter scale; the penetration depth of ultraviolet light is lower, at the micrometer scale), it can only act on the actuation parts in "sight" of the optical source and is also difficult for uniform control. Thus, light cannot be used in the enclosed space where the light is blocked; and even in open spaces, light also has trouble in actuating and processing thick and 3D-shaped objects, while magnetic field can penetrate almost any media deeply but failed at local and sequential control (*23*). Here, in our system, we developed a simple but competent strategy to achieve magnetically local and sequential control. As we characterized, under the same AMF with a constant H value, when the content of doped Fe_3O_4 NPs differs, their final stable temperature values are different as well; at the same time, T_i (the LC-isotropic phase transition temperature) is basically invariable with the contents of Fe_3O_4 NPs. Therefore, to trigger the actuation of different M-PULCEs, the required strengths of the magnetic field are different. That is to say, through rationally arranging different M-PULCEs in the desired regions achieved via AMF-assisted welding, we can control the movements of local positions by adjusting the intensity of AMF in the assembled actuator. For instance, the intensity of AMF (f = 320 kHz) for triggering the motion of the aligned M-PULCE-3 (reaching 120°C) is 163.08 Gs (H_1); for M-PULCE-2 and M-PULCE-1, the value is 219.27 Gs (H_2) and 283.15 Gs (H_3), respectively. Figure 5 (A and B) is an illustration of our strategy. To independently control the actuation of region A (made of M-PULCE-3), H_1 was set, and it can be seen that the two corresponding petals were closed; when the intensity was raised to H_2, region B (made of M-PULCE-2) responded sequentially; keep increasing the intensity to H_3, region C (made of M-PULCE-1) then was actuated. This is just similar to a series of logic switches: Region A corresponds to H_1, regions A and B correspond to H_2, and regions A, B, and C correspond to H_3. For example, if we want to separately control region B to put the petals down, we can simply input H_2 and then H_1. We also fabricated a locally controllable hand-like actuator (the preparation details can be found in Materials and Methods). With straightforward heating, all the "fingers" responded and bent (Fig. 5C); while by inputting different intensity signals of AMF, a series of localized motions were produced (Fig. 5D and movie S5). The content of magnetic NPs can be varied more with appropriate design to enlarge the control hierarchy. Also, in this work, we only adopted one LCE matrix with a fixed T_i. By regulating the molecular weight of the LC oligomer or cross-linking density, changing the LC monomer, spacer, or cross-linking agent, or other ways, T_i of the LCEs that can be adjusted to meet various application needs (*45*, *56*). It can be easily deduced that if LCEs with diverse T_i are used, then more sequences of motion portfolios can be devised. The degree of freedom of operations for magnetical control will be largely enriched.

Another improved level of magnetic control in our reprogrammable M-PULCEs is stepwise magnetic responsiveness, which comes from the supercritical behavior of nematic LCEs and the magneto-thermal responsiveness of M-PULCEs (*57*, *58*). Supercritical behavior is a continuous strain change over the broad nematic range such that a lot of intermediate motion states can be attained at the given temperature, enabling stepwise control. From XRD and DSC results, typical nematic phase was revealed in M-PULCEs (figs. S3 and S8). The stepwise motion controllability of M-PULCEs was tested and verified by segmented heating and cooling process (30° to 130°C) with a 10°C temperature interval (fig. S14; more experimental details can be found in Materials and Methods). On the basis of this, for the magneto-controlled robotic arm, except for a first-order ON/OFF

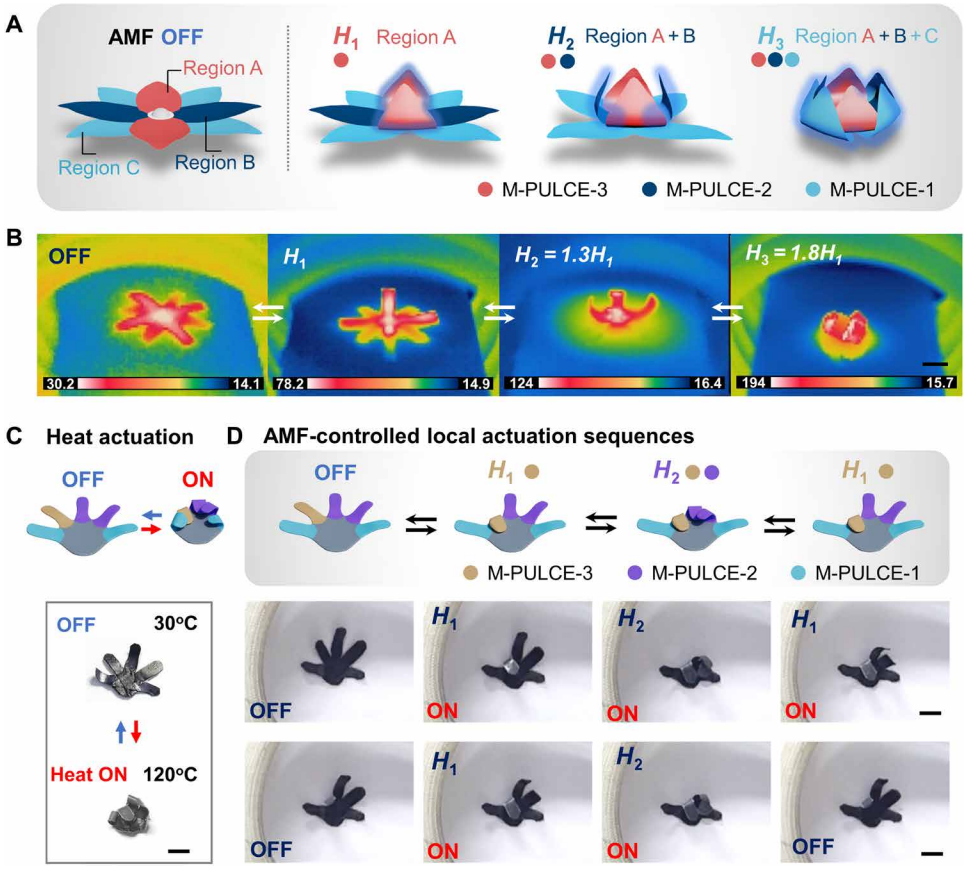

Fig. 5. Magnetically local and sequential control of M-PULCE actuators. (**A**) Schematic illustration of an eight-petal flower-shape actuator, which can be locally and sequentially controlled by different intensities of AMF. (**B**) IR thermal images of the flower-shape actuator under different intensities (*H*) of AMF. (**C**) Thermal actuation of a hand-shape actuator, showing a one-way ON/OFF actuation. (**D**) AMF-controlled local control of the hand-shape actuator with the input signal sequences of OFF-H_1-H_2-H_1-OFF-H_1-H_2-OFF. AMF conditions: f = 320 kHz, H_1 = 163.08 Gs, H_2 = 219.27 Gs (~1.3H_1), H_3 = 283.15 Gs (~1.8H_1). Scale bars, 10 mm.

transition (magnetic field ON, the temperature reaches T_i rapidly, arm up; magnetic field OFF, arm down) that we have already shown in Fig. 3A, we can stepwise control this process and intercept some parts by modulating the parameters of AMF (f = 495 kHz). As displayed in Fig. 6A, H was set to 132.59 Gs (corresponding temperature, 80°C), and the arm lifted to an angle of 14°; set to 141.80 Gs (100°C), the angle increased to 31°; by increasing H to 158.27 Gs (120°C), the angle reached the programmed maximum value (~60°). The instrument precision increased, and the tuning range can be larger, such as 5°C temperature interval or even 2°C temperature interval, by fine-tuning the intensity of AMF. This stepwise actuation process well simulates the multistage motion control of the traditional machine, but the actuator here is controlled wirelessly in sealed devices such as the robotic arm we displayed without any sophisticated circuits or sensors and can be applied.

It is worth mentioning that the M-PULCEs are responsive to not only heat and AMF but also light, since Fe_3O_4 NPs also exhibit a very strong photothermal effect under NIR (fig. S15). Programming, actuation, erasing, and reprogramming can all be achieved by these three stimuli according to different requirements. For example, taking the advantages of light, local erasure, and reprogramming of film-like actuators are achievable so as to partially encode new functions (fig. S16). Also, M-PULCE actuators can be simultaneously controlled by different stimuli (fig. S17). Moreover, the damaged M-PULCEs can be healed by both AMF and NIR via dynamic carbamate bond exchange (fig. S18). We found that AMF-assisted healing (efficiency: 91.1%, which was expressed as the percentage of the fracture stress of the healed film to that of the original one here) was more effective than NIR (efficiency: 35.7%) in our materials, which we speculated is because of the better-penetrating capability of AMF so that both the internal and the superficial areas can be reconnected via CAN. Figure 6B is a demonstration of AMF-assisted healing and reprogramming. The cut material was recovered under AMF, and then a bending while elongating motion was successfully installed in the healed sample by AMF. Besides, on the basis of the same bond exchange mechanism, the used or broken M-PULCE actuators can be remolded into a renewed 2D polydomain film with desired sizes by hot pressing (fig. S19), which is beneficial toward a sustainable society.

DISCUSSION

We explored the synergistic advantages of magnetothermal responsiveness and CAN in LCE actuators toward locally and sequentially controllable magnetic soft actuators with versatile reprogrammable contraction-based motion modes. Diverse motions including, but

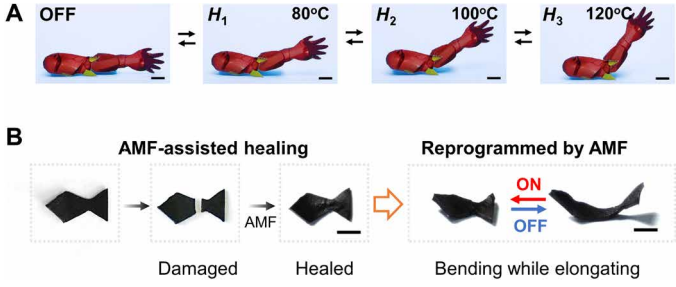

Fig. 6. Stepwise magnetic control of M-PULCE actuators and AMF-assisted healing and reprogramming. (**A**) Images of an M-PULCE actuator for raising "arms" under different intensities of AMF (f = 495 kHz, H_1 = 132.59 Gs, H_2 = 141.80 Gs, H_3 = 158.27 Gs). Scale bars, 10 mm. (**B**) A demonstration of AMF-assisted healing and reprogramming. The final healed and reprogrammed fish-like actuator performs a reversible bending while elongating motion in the AMF ON-OFF cycle. Scale bars, 5 mm. M-PULCE-2 was used for all the demonstrations in this figure.

not limited to, large-scale contraction, bidirectional shrinkage, dynamic patterns, and combined motions can be readily obtained and recomposed. Thanks to AMF-assisted welding, not only different motion modes but also chemically different materials can be assembled together to endow heterogeneous structures and multifunctionality. On one hand, we built monolithic multimaterial soft actuators such as floatable octopus-like actuators with a bulk foam body and a repeatedly deployable "satellite." On the other hand, by welding M-PULCEs with different contents of magnetic NPs, local control via magnetic fields that was very hard to realize in the past is feasible now. After the initial programming of the motions, various control sequences can be designed and written in for a great number of desired actuation modes. What is more is the fact that many other good performances are consolidated in our system. M-PULCE actuators can be magnetically stepwise-controlled, responded to multiple stimuli (programming, actuation, and reprogramming can be enabled by magnetic fields, heat, and light), healed under magnetic fields and NIR, and renewed by hot pressing. It should be noted that there are still a large number of functional combinations in this versatile system that are scarcely attained by other systems worth further and deeper exploring. The findings shown here are just the beginning.

Although the magnetic soft actuators presented here provide a sequence of promising features, on the flip side, the existence of thermal-responsive CAN (dynamic carbamate bonds) also compromise the high-temperature actuation stability to a certain extent. Yet, when the actuators are applied in a suitable temperature range and the long-period use time at excessively high temperatures is reduced, the actuation loss can be avoided. Nonetheless, the actuators here can be reprogrammed, which means that the actuation performances can still be restored even after being damaged. For all the magnetic soft actuators, although benefits such as various contraction-based morphing modes and local control are well created by our LCE system, since the magnetic actuation here is activated by AMF, it lacks the advantage regarding the movement mode changes brought about by the directionality of the magnetic field manifested in the hard-magnetic elastomeric actuators (*14*, *16*). What is more, in addition to LC alignment by mechanical forces and molding that we used in this work, is that other excellent methods and techniques such as surface alignment, compressive buckling, 3D printing, etc. can be used to create more complicated structures and micro-sized robots, the further application of which will surely open more opportunities (*33*–*35*). The great potential behind magnetic actuation and CAN-based LCE is waiting to be tapped further. With finer design and other advanced techniques incorporated, if the advantages can be combined, magnetic soft actuators with fully on-demand functionalities and architectures can be expected.

MATERIALS AND METHODS

Materials

RM82 (97%) was purchased from Shijiazhuang Sdynano Fine Chemicals. 1,3-Dimercaptopropane (98%) was purchased from Energy Chemical. 2-Mercaptoethanol (98%) and trimethylamine (98%) were purchased from TCI. Lysine triisocyanate (85%) was obtained from Zhengzhou JACS Chem Product Company. Hydrochloric acid (HCl, AR) was purchased from Beijing Tongguang Fine Chemicals. DBTDL (95%) and dichloromethane (DCM; 99.9%) were purchased from Adamas-beta. Sodium chloride (NaCl; >99.9%) was purchased from Shanghai Tian Scientific Company. Fe_3O_4 NPs (diameter: 20 nm) were purchased from Dalian Meilun Biological Technology Company. All the reagents were used directly without further purification. PU CANs and foams were fabricated following procedures described in the literature (*40*). The permanent magnet (made of NdFeB, size: 3.0 cm long × 2.0 cm wide × 0.5 cm thick) was purchased from Beijing HuaaoBio Company.

Synthesis of LC oligomer

Hydroxyl-terminated LC oligomer was synthesized following the procedures described in the literature (*44*). Excess RM82 (6.93 g, 10 mmol, 1 eq.) and 1,3-dimercaptopropane (0.936 g, 8.5 mmol, 0.85 eq.) were dissolved in 25 ml of DCM. Trimethylamine (5.15 g, 50 mmol) was then added to the mixture. The reactants were stirred overnight at room temperature. 2-Mercaptoethanol (3.59 g, 4.5 mmol) was added to react with the excess acrylate for 5 hours to form hydroxyl terminates. The reaction mixture was washed with HCl (1 N, 200 ml) and saturated solution of brine (200 ml). The mixture was concentrated under reduced pressure and dried in a vacuum oven at 50°C overnight. The oligomer was then obtained and used for the following procedures. The average molecular weight of the prepared LC-oligomer is ca. 4700 g/mol, calculated according to the integration ratio of $-CH_2$-OH alkyl protons (at A sites shown in fig. S1) at 3.95 parts per million (ppm) and phenyl protons (at B sites showing in fig. S1) at 8.15 ppm from the ^{1}H nuclear magnetic resonance (NMR) spectrum.

Synthesis of M-PULCEs and PULCEs

The fully cured polydomain M-PULCE samples were prepared by a classic "one-pot" reaction between hydroxyl and isocyanate. Hydroxyl-terminated LC-oligomer (0.47 g, 0.1 mmol, 1 eq.) and lysine triisocyanate (cross-linker) (0.031 g, 0.1 mmol, 0.1 eq.) were dissolved in 2 ml of DCM (the solvent should be used as little as possible to ensure that the system has relatively high viscosity). Different amounts of Fe_3O_4 NPs (5, 10, and 15 wt %) were added to the mixture, sonicated, and vigorously stirred on the vortex for 10 min to make sure of the even distribution. The samples without Fe_3O_4 NPs added are named as blank PULCEs. After that, 2 wt % DBTDL was added to initiate the crosslinking process. The mixture was stirred at room temperature, poured into a custom-made Teflon mold (4.0 cm long × 4.0 cm wide × 1.0 cm deep), reacted for 12 hours at 25°C, and

post–cross-linked for 3 hours at 100°C. After that, all the samples were immersed in DCM to extract soluble contents. The final polydomain M-PULCE and PULCE samples were obtained after drying in a vacuum oven at 30°C for 24 hours. The thickness of the M-PULCE sample used in this work is in the range of 0.12 to 1.55 mm. The sample thickness can be modulated by adjusting the total amount of monomers poured into the mold.

Preparation of monodomain PULCEs and M-PULCEs (thermal programming)

The uniaxial alignment was obtained by stretching the as-prepared polydomain M-PULCE or PULCE samples uniaxially to 130 to 180% strain (the stretching strain value determines the required actuation strain), and then the strain was fixed by Teflon tapes or clips (*59*). The samples were heated up to 150°C for 30 min to allow the dynamic covalent bond exchange so as to install the mesogen orientation.

Fabrication of various kinds of motions via heat

Bending

Bending motion can be realized by two methods. First, the polydomain sample was stretched to 130% strain and then winded around a large-diameter cylindrical mold for a half circle, the deformation of which was fixed by Teflon tapes, and the following step is the same as that in preparing monodomain samples. The final motion is unbending upon T_i while bending after cooling down. Second, bending motion can also be simply achieved by pasting a layer of Teflon tape on the monodomain sample to form a bilayer structure. The final motion is bending upon T_i while unbending after cooling down, which is an opposite process of the first method.

Spiraling while elongating

The polydomain sample was stretched to 180% strain and winded it around a cylindrical mold for several circles. The pitch of the spiral relies on the diameter of the mold used. The following step is the same as that in preparing monodomain samples. The coiling/uncoiling motion was fabricated by the similar process. The elongation rate can be adjusted by the stretching strain.

Twisting/uncoiling

This motion was attained by stretching the sample to 130% strain and twisting the strip. The rest of the procedure is the same as that in preparing monodomain samples.

Bidirectional shrinkage

The opposite apexes of a rectangular LCE sheet were stretched to 130 to 180% strain along the diagonal lines. Actuators with different shrinkage rates in two directions can be readily prepared by setting different tensile strains. The following step is the same as that in preparing monodomain samples.

3D convex

The convex was fabricated by a custom-built mold shown in Fig. 3C. Other kinds of active patterns can also be encoded by using suitable molds.

Dynamic patterns

The dynamic patterns were obtained by using iron hollow molds with the desired patterns. An LCE sheet was placed on the mold. The mold and sheet were sandwiched between two thin Teflon films, and the whole was pressed between two hot plates (150°C). The depth of the pattern on M-PULCEs depends on the value of the pressure.

AMF-assisted programming of M-PULCEs

This programming process is enabled by just replacing the heating step with a magnetic processing step. Under a certain condition of AMF, magnetothermal effect makes the whole sample heat up above 150°C (the temperature was adjusted by controlling the intensity of AMF and measured by an IR camera). The deformed samples were placed in the magnetic field for 5 min to fix the alignment. The magnetic programming time is significantly shorter than direct heating, which is because the existence of Fe_3O_4 NPs inside M-PULCEs reduces the heat loss originating from heat transfer and thermal diffusion, improving the efficiency of dynamic bond exchange.

Light-assisted programming of M-PULCEs

NIR source with a wavelength of 808 nm was used. The light programming process was achieved by substituting the heating step by shining NIR on the deformed sample. The NIR intensity of NIR was regulated to make the temperature of the surface of the sample increase above 150°C (the temperature was measured by an IR camera). The sample was irradiated for 5 min to install alignment.

Reprogramming and erasing the motions of M-PULCEs

Reprogramming

Reprogramming is achieved by directly deforming the aligned M-PULCE into another desired shape and then encoding the alignment via the completely same procedures described in the "Programming" section by heat, magnetics, or light.

Erasing

If the programmed motion needs to be erased, i.e., back to the polydomain state, then it is only required to put the sample in an environment of 150°C without applying any external force, which can be realized by direct heating, AMF, and NIR. Erasing process often requires a longer time than reprogramming, as bond exchange is relatively slower in the stress-free sample (*60*).

AMF-assisted welding

Basic welding process

Two pieces of M-PULCEs were partially overlapped. The resulting sample was fixed by Teflon tapes to keep the surface contact. They were placed under a certain intensity of AMF to allow dynamic carbamate bond exchange and bond the contact areas together covalently, leading to samples being welded seamlessly. A total of 150°C (detected with an IR camera) for 5 min is enough for effective welding. Blank PULCEs or PU CANs can also be welded with M-PULCEs. The procedures are the same as above. The welded structures shown in this work are all achieved by AMF-assisted welding.

Welding aligned actuators

An M-PULCE strip with higher contents of Fe_3O_4 NPs was used as the welding solder. For example, in this work, to weld actuators made of M-PULCE-1 or M-PULCE-2, M-PULCE-3 can be used as the solder. When M-PULCE-3 reaches 150°C, the inner temperature of M-PULCE-1 or M-PULCE-2 is lower, and bond exchange is slow such that the programmed alignment will not be damaged in the time scale of the welding process (5 min). Bond exchange is activated only in the contact areas of M-PULCE-1 or M-PULCE-2 with M-PULCE-3 because of heat conduction.

Preparation of the Mobius ring

One end of a monodomain M-PULCE-2 was given a half-twist and joined with the other end. The two ends were welded by using an M-PULCE-3 solder placed in between the two ends. They were welded together by AMF according to the same procedures we described above.

Preparation of the trefoil knot

One end of a monodomain M-PULCE-2 was turned over three times and then welded to the other by an M-PULCE-3 solder placed in between the two ends. They were welded together by AMF according to the same procedures we described above.

Preparation of the satellite-like actuator

The actuator was prepared by welding while programming. A polydomain M-PULCE-2 strip was stretched to 50% strain, and the two ends were fixed by Teflon tapes on a glass slide. Two pieces of PU CANs were placed and overlapped upon the M-PULCE strip. They were welded together by AMF according to the same procedures we described above. A layer of Teflon tape was then pasted with the monodomain sample on the back (the nonwelded side) for bending motions. The thickness of the PU CAN used here is 0.45 mm.

Preparation of the octopus-like actuator

The actuator was prepared by welding after programming. Eight pieces of M-PULCE-1 were programmed with bending/unbending or rolling/straightening motions. These samples were placed and fixed on a glass slide by Teflon tapes, but the areas that need to be welded are left exposed. A piece of M-PULCE-3 was served as the solder and placed on the area, while the PU foam was put upon the solder. The structure was fixed by Teflon tapes. They were welded together by AMF according to the same procedures we described above. The thickness of the PU foam is 8.95 mm.

Preparation of the flower-shape and hand-shape actuators that can be sequentially controlled by AMF

The actuator was prepared by welding while programming. Polydomain M-PULCEs with different content of Fe_3O_4 NPs were arranged at the required regions with partial area overlapped. The overlapped region was fixed on a glass side by Teflon tapes. Each "arm" was then stretched to 150% strain, and the deformation was also fixed by tapes. The M-PULCEs were then chemically welded and programmed. A layer of Teflon tape was then pasted on the back of the actuator for reversible bending motions.

Gel content tests

A series of PULCE and M-PULCE samples were soaked in DCM for 3 days with the solvent being refreshed daily. Afterward, the residual polymer samples were dried at 30°C in a vacuum oven until the weight reached a constant value. The gel content was calculated as the weight ratio of the polymer after and before the solvent extraction. Each value was the average of three repeated tests.

Swelling experiments of the welded samples

The swelling experiments for the welded M-PULCEs and composites were conducted in DCM for 12 hours. The sample was then taken from the solvent carefully and dried at room temperature slowly.

Stepwise control experiments

A free-standing monodomain M-PULCE sample was subjected to a segmented heating and cooling process (30° to 130°C) with a 10°C temperature interval on a precise hot stage. Each temperature was held for 20 min. The length of the actuator was measured at each temperature then. The stability of the intermediate states was further tested by measuring the strain at the given temperature (80°, 90°, 100°, and 110°C) every 5 min within 20 min.

Local erasure and reprogramming by NIR

The combination of multiple stimuli to achieve local control and programming/reprogramming of the actuator will effectively improve the functionality of the actuator and help to study the synergy of multiple stimuli. M-PULCE has a strong photothermal effect that can reach the temperature required for activating the dynamic exchange reaction (fig. S14). Therefore, the alignment of the M-PULCE and the resultant locomotion can be locally erased and reprogrammed by NIR. As shown in fig. S15, we prepared a spiral spline, which can realize a deformation between spiraling and uncoiling under the action of AMF. Use a mask to cover the right side of the spline and then irradiate the spline with an 808-nm laser for 20 min (at around 150°C observed from IR thermal camera). It could be found that the left side of the spline is unwound. When the laser is removed, the left side remains unwound (i.e., the alignment of LCs is erased). At this time, AMF is applied again, only the right side of the spline was driven, and the left side did not change. Then, covering the right side of the spline with a mask again, we stretched the edge of the left spline, spiraled it with a smaller pitch than that of the right side, fixed it on the glass slide with polytetrafluoroethylene tapes, and irradiated the spline with an 808-nm laser for 5 min. After removing the laser, it is found that the left sample became spiral again. When an AMF was applied, both the left and right sides of the spline could be driven to uncoil.

Self-healing by NIR and AMF

For self-healing by NIR and AMF, M-PULCE strips were cut by a razor blade for a 2-mm incision. The cut samples were either put into AMF (f = 495 kHz) or irradiated by an 808-nm laser for 5 min (at around 150°C observed from IR thermal camera). The healing efficiency was calculated by the recovery percentage of the tensile stress at break.

Remolding

The M-PULCEs with the same constituent were cut into pieces, then placed in the mold with desired shapes, and hot-pressed at 160°C for 2 hours under a pressure of 10 MPa. After cooling down, a renewed polydomain film was obtained.

NIR penetrability tests

PU films (insensitive to NIR; thickness: 1.75 mm) and thin tinfoil (thickness: 20 μm) were used for the tests. The PU film was placed on the top of an M-PULCE-2 sample (thickness: 0.25 mm). The NIR laser (wavelength: 808 nm) with the intensity of 0.55 W/cm^2 was shined on the PU film. After 180 s, the detected temperature of M-PULCE-2 was around 87°C. Without the PU film, under the same NIR condition, the temperature of M-PULCE-2 reached 156°C within 20 s. The NIR laser with higher intensity (0.80 W/cm^2) irradiated on very thin tinfoil (totally opaque, thickness: 20 μm) and the M-PULCE-2 film was under the tinfoil, and there was no temperature raising detected on the M-PULCE.

Experimental and characterization apparatus

^{1}H NMR spectrum (400 MHz; Chloroform-D) was performed on a JEOL ECX-400 spectrometer. DSC was conducted using a TA-Q2000 DSC instrument at a scanning rate of 10°C/min. Stress relaxation tests were conducted by a TA-Q800 dynamic mechanical analysis (DMA) apparatus in the tension film geometry with a constant strain of 10% for all the materials as we monitored the stress relaxation

over time. Uniaxial tensile tests of PU foams and welded PU foam/M-PULCE composites were conducted by DMA with a force rate of 0.5 N/min. Uniaxial tensile tests of all the other materials were conducted by an Instron 3342 universal mechanical testing machine with a speed rate of 20 mm/min. The thermal weight loss was measured using a TA-Q50 thermal gravity analysis under nitrogen atmosphere at a heating rate of 20°C/min. POM was measured using a Nikon Eclipse LV100POL polarizing optical microscope with crossed polarizers. XRD tests were performed using a Bruker D8 Discover diffractometer.

The AMF device was supplied by Shuangping Instrument Technology (frequency f = 495 and 320 kHz with adjustable field intensity). For all the programming, welding, healing, and reprogramming, the AMF device with f = 495 kHz was used; for the magnetic actuation, the device with f = 320 kHz and f = 495 kHz were both used. NIR laser source (wavelength: 808 nm) was purchased from HI-Tech Optoelectronics Co. Ltd. The intensity was measured by an optical power meter. The temperature was measured by an IR thermal imaging camera (FLIR E40).

SUPPLEMENTARY MATERIALS

Supplementary material for this article is available at https://science.org/doi/10.1126/sciadv.abo6021

REFERENCES AND NOTES

1. N. Ebrahimi, C. Bi, D. J. Cappelleri, G. Ciuti, A. T. Conn, D. Faivre, N. Habibi, A. Hošovský, V. Iacovacci, I. S. M. Khalil, V. Magdanz, S. Misra, C. Pawashe, R. Rashidifar, P. E. D. Soto-Rodriguez, Z. Fekete, A. Jafari, Magnetic actuation methods in bio/soft robotics. *Adv. Funct. Mater.* **31**, 2005137 (2021).
2. M. Li, A. Pal, A. Aghakhani, A. Pena-Francesch, M. Sitti, Soft actuators for real-world applications. *Nat. Rev. Mater.* **7**, 235–249 (2022).
3. Z. Ren, W. Hu, X. Dong, M. Sitti, Multi-functional soft-bodied jellyfish-like swimming. *Nat. Commun.* **10**, 2703–2724 (2019).
4. W. Hu, G. Z. Lum, M. Mastrangeli, M. Sitti, Small-scale soft-bodied robot with multimodal locomotion. *Nature* **554**, 81–85 (2018).
5. Y. Kim, H. Yuk, R. Zhao, S. A. Chester, X. Zhao, Printing ferromagnetic domains for untethered fast-transforming soft materials. *Nature* **558**, 274–279 (2018).
6. J. Cui, T. Y. Huang, Z. Luo, P. Testa, H. Gu, X. Z. Chen, B. J. Nelson, L. J. Heyderman, Nanomagnetic encoding of shape-morphing micromachines. *Nature* **575**, 164–168 (2019).
7. H. F. Lu, M. Wang, X. M. Chen, B. P. Lin, H. Yang, Interpenetrating liquid-crystal polyurethane/polyacrylate elastomer with ultrastrong mechanical property. *J. Am. Chem. Soc.* **141**, 14364–14369 (2019).
8. D. Tang, C. Zhang, H. Sun, H. Dai, J. Xie, J. Fu, P. Zhao, Origami-inspired magnetic-driven soft actuators with programmable designs and multiple applications. *Nano Energy* **89**, 106424 (2021).
9. Q. Ze, X. Kuang, S. Wu, J. Wong, S. M. Montgomery, R. Zhang, J. M. Kovitz, F. Yang, H. J. Qi, R. Zhao, Magnetic shape memory polymers with integrated multifunctional shape manipulation. *Adv. Mater.* **32**, 1906657 (2020).
10. J. A.-C. Liu, J. H. Gillen, S. R. Mishra, B. A. Evans, J. B. Tracy, Photothermally and magnetically controlled reconfiguration of polymer composites for soft robotics. *Sci. Adv.* **5**, eaaw2897 (2019).
11. L. Wang, M. Y. Razzaq, T. Rudolph, M. Heuchel, U. Nöchel, U. Mansfeld, Y. Jiang, O. E. C. Gould, M. Behl, K. Kratz, A. Lendlein, Reprogrammable, magnetically controlled polymeric nanocomposite actuators. *Mater. Horiz.* **5**, 861–867 (2018).
12. H. Deng, K. Sattari, Y. Xie, P. Liao, Z. Yan, J. Lin, Laser reprogramming magnetic anisotropy in soft composites for reconfigurable 3D shaping. *Nat. Commun.* **11**, 6325–6334 (2020).
13. L. Cao, D. Yu, Z. Xia, H. Wan, C. Liu, T. Yin, Z. He, Ferromagnetic liquid metal putty-like material with transformed shape and reconfigurable polarity. *Adv. Mater.* **32**, 2000827 (2020).
14. Y. Alapan, A. C. Karacakol, S. N. Guzelhan, I. Isik, M. Sitti, Reprogrammable shape morphing of magnetic soft machines. *Sci. Adv.* **6**, eabc6414 (2020).
15. H. Song, H. Lee, J. Lee, J. K. Choe, S. Lee, J. Y. Yi, S. Park, J. W. Yoo, M. S. Kwon, J. Kim, Reprogrammable ferromagnetic domains for reconfigurable soft magnetic actuators. *Nano Lett.* **20**, 5185–5192 (2020).
16. X. Kuang, S. Wu, Q. Ze, L. Yue, Y. Jin, S. M. Montgomery, F. Yang, H. J. Qi, R. Zhao, Magnetic dynamic polymers for modular assembling and reconfigurable morphing architectures. *Adv. Mater.* **33**, 2102113 (2021).
17. M. O. Saed, A. Gablier, E. M. Terentjev, Exchangeable liquid crystalline elastomers and their applications. *Chem. Rev.* **122**, 4927–4945 (2022).
18. B. Yang, R. Baines, D. Shah, S. Patiballa, E. Thomas, M. Venkadesan, R. Kramer-Bottiglio, Reprogrammable soft actuation and shape-shifting via tensile jamming. *Sci. Adv.* **7**, eabh2073 (2021).
19. S. M. Mirvakili, I. W. Hunter, Artificial muscles: Mechanisms, applications, and challenges. *Adv. Mater.* **30**, 1704407 (2018).
20. S. M. Mirvakili, D. Sim, I. W. Hunter, R. Langer, Actuation of untethered pneumatic artificial muscles and soft robots using magnetically induced liquid-to-gas phase transitions. *Sci. Robot.* **5**, eaaz4239 (2020).
21. J. Ma, Y. Yang, C. Valenzuela, X. Zhang, L. Wang, W. Feng, Mechanochromic, shape-programmable and self-healable cholesteric liquid crystal elastomers enabled by dynamic covalent boronic ester bonds. *Angew. Chem. Int. Ed.* **61**, e202116219 (2022).
22. X. Pang, L. Qin, B. Xu, Q. Liu, Y. Yu, Ultralarge contraction directed by light-driven unlocking of prestored strain energy in linear liquid crystal polymer fibers. *Adv. Funct. Mater.* **30**, 2002451 (2020).
23. Z. C. Jiang, Y. Y. Xiao, Y. Zhao, Shining light on liquid crystal polymer networks: Preparing, Reconfiguring, and driving soft actuators. *Adv. Opt. Mater.* **7**, 1900262 (2019).
24. Y. Chen, J. Yang, X. Zhang, Y. Feng, H. Zeng, L. Wang, W. Feng, Light-driven bimorph soft actuators: Design, fabrication, and properties. *Mater. Horiz.* **8**, 728–757 (2021).
25. M. Sitti, D. S. Wiersma, Pros and cons: Magnetic versus optical microrobots. *Adv. Mater.* **32**, 1906766 (2020).
26. C. Ohm, M. Brehmer, R. Zentel, Liquid crystalline elastomers as actuators and sensors. *Adv. Mater.* **22**, 3366–3387 (2010).
27. T. H. Ware, M. E. McConney, J. J. Wie, V. P. Tondiglia, T. J. White, Voxelated liquid crystal elastomers. *Science* **347**, 982–984 (2015).
28. T. J. White, D. J. Broer, Programmable and adaptive mechanics with liquid crystal polymer networks and elastomers. *Nat. Mater.* **14**, 1087–1098 (2015).
29. H. Yang, A. Buguin, J.-M. Taulemesse, K. Kaneko, S. Méry, A. Bergeret, P. Keller, Micron-sized main-chain liquid crystalline elastomer actuators with ultralarge amplitude contractions. *J. Am. Chem. Soc.* **131**, 15000–15004 (2009).
30. Q. He, Z. Wang, Y. Wang, A. Minori, M. T. Tolley, S. Cai, Electrically controlled liquid crystal elastomer–based soft tubular actuator with multimodal actuation. *Sci. Adv.* **5**, eaax5746 (2019).
31. Z. Pei, Y. Yang, Q. Chen, E. M. Terentjev, Y. Wei, Y. Ji, Mouldable liquid-crystalline elastomer actuators with exchangeable covalent bonds. *Nat. Mater.* **13**, 36–41 (2014).
32. B. Jin, J. Liu, Y. Shi, G. Chen, Q. Zhao, S. Yang, Solvent-ASSISTED 4D programming and reprogramming of liquid crystalline organogels. *Adv. Mater.* **34**, 2107855 (2022).
33. C. L. Van Oosten, C. W. M. Bastiaansen, D. J. Broer, Printed artificial cilia from liquid-crystal network actuators modularly driven by light. *Nat. Mater.* **8**, 677–682 (2009).
34. A. Kotikian, R. L. Truby, J. W. Boley, T. J. White, J. A. Lewis, 3D printing of liquid crystal elastomeric actuators with spatially programed nematic order. *Adv. Mater.* **30**, 1706164 (2018).
35. Y. Li, H. Yu, K. Yu, X. Guo, X. Wang, Reconfigurable three-dimensional mesotructures of spatially programmed liquid crystal elastomers and their ferromagnetic composites. *Adv. Funct. Mater.* **31**, 2100338 (2021).
36. A. Kaiser, M. Winkler, S. Krause, H. Finkelmann, A. M. Schmidt, Magnetoactive liquid crystal elastomer nanocomposites. *J. Mater. Chem.* **19**, 538–543 (2009).
37. J. M. Haberl, A. Sanchez-Ferrer, A. M. Mihut, H. Dietsch, A. M. Hirt, R. Mezzenga, Liquid-crystalline elastomer-nanoparticle hybrids with reversible switch of magnetic memory. *Adv. Mater.* **25**, 1787–1791 (2013).
38. J. Zhang, Y. Guo, W. Hu, M. Sitti, Wirelessly actuated thermo- and magneto-responsive soft bimorph materials with programmable shape-morphing. *Adv. Mater.* **33**, 2100336 (2021).
39. J. Zhang, Y. Guo, W. Hu, R. H. Soon, Z. S. Davidson, M. Sitti, Liquid crystal elastomer-based magnetic composite films for reconfigurable shape-morphing soft miniature machines. *Adv. Mater.* **33**, 2006191 (2021).
40. S. Zhang, Y. Zhang, Y. Wu, Y. Yang, Q. Chen, H. Liang, Y. Wei, Y. Ji, A magnetic solder for assembling bulk covalent adaptable network blocks. *Chem. Sci.* **11**, 7694–7700 (2020).
41. R. Mohr, K. Kratz, T. Weigel, M. Lucka-Gabor, M. Moneke, A. Lendlein, Initiation of shape-memory effect by inductive heating of magnetic nanoparticles in thermoplastic polymers. *Proc. Natl. Acad. Sci. U.S.A.* **103**, 3540–3545 (2006).
42. S.-h. Noh, S. H. Moon, T.-H. Shin, Y. Lim, J. Cheon, Recent advances of magneto-thermal capabilities of nanoparticles: From design principles to biomedical applications. *Nano Today* **13**, 61–76 (2017).
43. N. Zheng, Z. Fang, W. Zou, Q. Zhao, T. Xie, Thermoset shape-memory polyurethane with intrinsic plasticity enabled by transcarbamoylation. *Angew. Chem. Int. Ed.* **55**, 11421–11425 (2016).
44. Z. Wen, M. K. McBride, X. Zhang, X. Han, A. M. Martinez, R. Shao, C. Zhu, R. Visvanathan, N. A. Clark, Y. Wang, K. Yang, C. N. Bowman, Reconfigurable LC elastomers: Using

a thermally programmable monodomain to access two-way free-standing multiple shape memory polymers. *Macromolecules* **51**, 5812–5819 (2018).
45. Y. Zhang, Z. Wang, Y. Yang, Q. Chen, X. Qian, Y. Wu, H. Liang, Y. Xu, Y. Wei, Y. Ji, Seamless multimaterial 3D liquid-crystalline elastomer actuators for next-generation entirely soft robots. *Sci. Adv.* **6**, eaay8606 (2020).
46. Y. Wu, Y. Yang, Q. Chen, X. Qian, Y. Wei, Y. Ji, Liquid crystalline soft actuators with switchable thermal reprogrammability. *Angew. Chem. Int. Ed.* **59**, 4778–4784 (2020).
47. R. Yang, Y. Zhao, Non-uniform optical inscription of actuation domains in a liquid crystal polymer of uniaxial orientation: An approach to complex and programmable shape changes. *Angew. Chem. Int. Ed.* **56**, 14202–14206 (2017).
48. H. J. Bae, S. Bae, C. Park, S. Han, J. Kim, L. N. Kim, K. Kim, S. H. Song, W. Park, S. Kwon, Biomimetic microfingerprints for anti-counterfeiting strategies. *Adv. Mater.* **27**, 2083–2089 (2015).
49. M. Ilami, H. Bagheri, R. Ahmed, E. O. Skowronek, H. Marvi, Materials, actuators, and sensors for soft bioinspired robots. *Adv. Mater.* **33**, 2003139 (2021).
50. B. Han, Z.-C. Ma, Y.-L. Zhang, L. Zhu, H. Fan, B. Bai, Q.-D. Chen, G.-Z. Yang, H.-B. Sun, Reprogrammable soft robot actuation by synergistic magnetic and light fields. *Adv. Funct. Mater.* **32**, 2110997 (2021).
51. X. Cheng, Y. Zhang, Micro/Nanoscale 3D assembly by rolling, folding, curving, and buckling approaches. *Adv. Mater.* **31**, 1901895 (2019).
52. Y. Guo, J. Zhang, W. Hu, M. T. A. Khan, M. Sitti, Shape-programmable liquid crystal elastomer structures with arbitrary three-dimensional director fields and geometries. *Nat. Commun.* **12**, 5936–5944 (2021).
53. M. A. Skylar-Scott, J. Mueller, C. W. Visser, J. A. Lewis, Voxelated soft matter via multimaterial multinozzle 3D printing. *Nature* **575**, 330–335 (2019).
54. Y. Liu, B. Shaw, M. D. Dickey, J. Genzer, Sequential self-folding of polymer sheets. *Sci. Adv.* **3**, e1602417 (2017).
55. X. Wang, X. Guo, J. Ye, N. Zheng, P. Kohli, D. Choi, Y. Zhang, Z. Xie, Q. Zhang, H. Luan, K. Nan, B. H. Kim, Y. Xu, X. Shan, W. Bai, R. Sun, Z. Wang, H. Jang, F. Zhang, Y. Ma, Z. Xu, X. Feng, T. Xie, Y. Huang, Y. Zhang, J. A. Rogers, Freestanding 3D mesostructures, functional devices, and shape-programmable systems based on mechanically induced assembly with shape memory polymers. *Adv. Mater.* **31**, 1805615 (2019).
56. Z. Pei, Y. Yang, Q. Chen, Y. Wei, Y. Ji, Regional shape control of strategically assembled multishape memory vitrimers. *Adv. Mater.* **28**, 156–160 (2016).
57. A. Lebar, Z. Kutnjak, S. Žumer, H. Finkelmann, A. Sánchez-Ferrer, B. Zalar, Evidence of supercritical behavior in liquid single crystal elastomers. *Phys. Rev. Lett.* **94**, 197801 (2005).
58. Q. Chen, W. Li, Y. Wei, Y. Ji, Reprogrammable 3D liquid-crystalline actuators with precisely controllable stepwise actuation. *Adv. Intell. Syst.* **3**, 2000249 (2021).
59. Q. Chen, Y. Li, Y. Yang, Y. Xu, X. Qian, Y. Wei, Y. Ji, Durable liquid-crystalline vitrimer actuators. *Chem. Sci.* **10**, 3025–3030 (2019).
60. Y. Yang, E. M. Terentjev, Y. Zhang, Q. Chen, Y. Zhao, Y. Wei, Y. Ji, Reprocessable thermoset soft actuators. *Angew. Chem. Int. Ed.* **58**, 17474–17479 (2019).

Acknowledgments

Funding: This research was supported by the National Natural Science Foundation of China (nos. 51722303, 21674057, and 21788102). **Author contributions:** Y. Wu and S.Z. contributed equally to this work. Y.J., S.Z., and Y. Wu conceived the central idea. Y. Wu and S.Z. performed the main experiments. Y. Wu, S.Z., Y.Y., and Z.L. analyzed the results. S.Z., Y. Wu, and Y.J. wrote the manuscript draft together. All authors reviewed and edited the manuscript. Y.J. and Y.We. arranged the funding and infrastructure for the project. **Competing interests:** The authors declare that they have no competing interests. **Data and materials availability:** All data needed to evaluate the conclusions in the paper are present in the paper and/or the Supplementary Materials.

Submitted 14 February 2022
Accepted 10 May 2022
Published 24 June 2022
10.1126/sciadv.abo6021